ESTIMATION OF EFFECTIVE MASSES AND INTERFACE LOADS BY COMPLEMENTARY VIBRATION TEST

R. Arena [(1)], M. Giuliano [(1)], N. Girault [(1)], N. Roy [(2)]

[(1)] *Thales Alenia Space, 5 Allée des Gabians, 06150 Cannes, France, Email: roberto.arena@thalesaleniaspace.com*
[(2)] *Top Modal, 130 rue Galilée, 31670 Labège, France, Email : nicolas.roy@topmodal.fr*

ABSTRACT

Effective masses and interface loads play a fundamental role in the context of the sine testing of a Spacecraft. In some cases, loads must be evaluated at the interface of an internal subsystem if equivalent quasi-static accelerations have to be monitored in order to not exceed design loads.
Recently an alternative approach to determining experimentally effective masses has been developed by Thales Alenia Space and Top Modal. Using this effective mass, loads at Spacecraft and Subsystem interfaces can be evaluated if specific conditions are fulfilled. The theoretical background behind the entire method is presented as well as the numerical simulations done to validate it. Experimental validation has been carried out on a simple test case consisting of a clamped beam with a tip mass and on two main subsystems of an Instrument developed and successfully tested by Thales Alenia Space.

1. INTRODUCTION

Effective masses can be obtained from base excitation sine and random vibration tests using one of several well-known techniques such as the use of load cells (FMD), strain gages, coil current and the mass operator method. Each of these techniques has its advantages and drawbacks.
Recently an alternative approach to determining effective masses has been developed by Thales Alenia Space and Top Modal. This approach involves performing an additional vibration test using a small shaker or impact hammer while taking advantage of the instrumentation used for the base excitation test. This additional test provides the effective flexibilities which combined with the effective transmissibilities of the base excitation test through a simple formula, lead to the effective masses of the spacecraft.
In some cases, the effective masses and loads must be evaluated at the interface of an internal subsystem if equivalent quasi-static accelerations have to be monitored during the test in order to not exceed design loads. The conditions under which loads at the spacecraft interface can be considered as acting directly at subsystem interface are described. It is shown that these conditions may be satisfied in the case of a resonant subsystem which is weakly coupled with the remaining spacecraft structure.

The background theory is first presented starting with a brief review of the modal approach including frequency response functions (FRF) and modal effective parameters (MEP). Existing methods for obtaining effective masses are discussed followed by a presentation of the new method.
The elaboration of the interface loads, at both system and subsystem levels, is presented along with the assumptions used to establish the relationship between the two. A numerical simulation is used to illustrate and validate the approach.
Finally, the experimental validation of the effective masses obtained through a complementary vibration test, as well as the validation of the subsystem loads, which was performed on a simple test case and a spacecraft instrument.
The main results are presented and the lessons learned are discussed in the aim of identifying potential problems and suggesting solutions for future applications.

2. THEORY

2.1 Frequency Response Functions

Consider the discretized structure shown in Fig. 1 with *j* junction DOF and *i* internal DOF subjected to prescribed motion at the junction and/or internal forces.

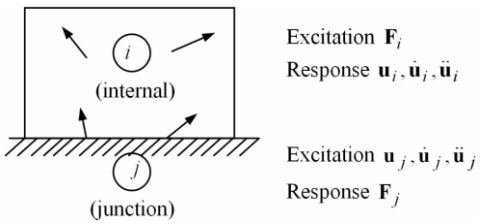

Figure 1 : Structural DOF

In the frequency domain, the relationship between the excitations and the responses can be expressed in terms of the following FRF :

$$\begin{bmatrix} \mathbf{u}_i(\omega) \\ \mathbf{F}_j(\omega) \end{bmatrix} = \begin{bmatrix} \mathbf{G}_{ii}(\omega) & \mathbf{T}_{ij}(\omega) \\ -\mathbf{T}_{ji}(\omega) & \mathbf{K}_{jj}(\omega) \end{bmatrix} \begin{bmatrix} \mathbf{F}_i(\omega) \\ \mathbf{u}_j(\omega) \end{bmatrix} \quad (1)$$

where **G**, **T** and **K** are the dynamic flexibility, transmissibility and stiffness matrices respectively. See [1] for further details.

The above FRF can be defined using a modal approach where the internal motion of the structure is written as the sum of motion induced by the junction and the motion expressed in the basis of constrained junction normal modes

$$\mathbf{u}_i = \mathbf{\Psi}_{ij}\mathbf{u}_j + \mathbf{\Phi}_{ik}\mathbf{q}_k \tag{2}$$

where $\mathbf{\Psi}$ is the matrix of static constraint modes and $\mathbf{\Phi}$ is the matrix of normal modes given by:

$$\mathbf{\Psi}_{ij} = -\mathbf{K}_{ii}^{-1}\mathbf{K}_{ij} \tag{3}$$

$$(-\omega_k^2\mathbf{M}_{ii} + \mathbf{K}_{ii})\mathbf{\Phi}_{ik} = \mathbf{0} \tag{4}$$

Applying the transformation of Eq. (2) leads to the following expressions for the FRF:

$$\mathbf{G}_{ii}(\omega) = \sum_{k=1}^{n} H_k(\omega)\,\tilde{\mathbf{G}}_{ii,k} \tag{5}$$

$$\mathbf{T}_{ij}(\omega) = \sum_{k=1}^{n} T_k(\omega)\,\tilde{\mathbf{T}}_{ij,k} - \mathbf{M}_{ii}^{-1}\mathbf{M}_{ij} \tag{6}$$

$$\mathbf{K}_{jj}(\omega) = -\omega^2\,\mathbf{M}_{jj}(\omega) + \bar{\mathbf{K}}_{jj} \tag{7}$$

where $\mathbf{M}_{jj}(\omega)$ is the dynamic mass matrix given by:

$$\mathbf{M}_{jj}(\omega) = \sum_{k=1}^{n} T_k(\omega)\,\tilde{\mathbf{M}}_{jj,k} + \mathbf{M}_{jj} - \mathbf{M}_{ji}\mathbf{M}_{ii}^{-1}\mathbf{M}_{ij} \tag{8}$$

H_k and T_k are the amplification and transmissibility factors of mode k and are a function of the circular frequency ω_k and viscous damping ratio ζ_k:

$$H_k(\omega) = \frac{1}{1-(\omega/\omega_k)^2 + i\,2\,\zeta_k(\omega/\omega_k)} \tag{9}$$

$$T_k(\omega) = \frac{1+i\,2\,\zeta_k(\omega/\omega_k)}{1-(\omega/\omega_k)^2 + i\,2\,\zeta_k(\omega/\omega_k)} \tag{10}$$

2.2 Modal Effective Parameters

The three FRF matrices **G**, **T** and **M** have the same basic form expressing the contribution of each mode as the product of an amplification factor and a matrix of terms independent of ω known as the modal effective parameters where

$$\tilde{\mathbf{G}}_{ii,k} = \frac{\mathbf{\Phi}_{ik}\,\mathbf{\Phi}_{ki}}{\omega_k^2\,m_k} \tag{11}$$

$$\tilde{\mathbf{T}}_{ij,k} = \frac{\mathbf{\Phi}_{ik}\,\mathbf{L}_{kj}}{m_k} \tag{12}$$

$$\tilde{\mathbf{M}}_{jj,k} = \frac{\mathbf{L}_{jk}\,\mathbf{L}_{kj}}{m_k} \tag{13}$$

are the effective flexibility, transmissibility and mass matrices of mode *k*. These effective parameters are independent of the normalization of the eigenvectors and have the same dimension and units as the corresponding FRF.

In the above expressions, m_k is the generalized mass of mode *k* and $\mathbf{L}_{kj}$ is the matrix of participation factors defined by:

$$\mathbf{L}_{kj} = \mathbf{\Phi}_{ki}(\mathbf{M}_{ii}\,\mathbf{\Psi}_{ij} + \mathbf{M}_{ij}) \tag{14}$$

2.3 Effective Mass Estimation

The dynamic mass of the spacecraft is of particular importance in the context of coupled analysis with the launch vehicle. Using mode superposition, the dynamic mass of Eq. (8) is expressed in terms of the effective masses which play a fundamental role in primary notching. Effective masses can be derived from base excitation sine and random vibration tests if forces at the interface are available since they are obtained from the ratio force/acceleration. Several techniques summarized in Fig. 2 may be used to obtain effective masses.

Method	Advantages	Drawbacks
Load Cells (FMD)	- Accuracy	- Added mass and flexibility of test fixture at interface - Limited availability
Strain Gages	- Simple setup	- Difficulties with calibration and sensitivity
Coil Current (electrodynamic shaker)	- No test fixture required	- Single force measurement along excitation direction - Influence of mobile mass of shaker - Limited accuracy
Mass Operator	- Requires only acceleration measurements	- Finite element model required - Accuracy depends on quality of FE model

Figure 2 : Force Measurement Techniques

Direct measurement of the interface forces using load cells provides accurate results but can produce added mass and flexibility to the test fixture. Strain gages are less intrusive and relatively simple to install, but may produce less accurate results due to difficulties with calibration and sensitivity. Use of the coil current requires no text fixture, however accuracy is in general poor and only a single force along the excitation direction is available.

The mass operator method combines the measured accelerations with the mass matrix of the finite element model condensed statically (Guyan) on the same set of sensors.

The interface loads $\mathbf{F}_j$ are recovered by multiplying the condensed mass matrix $\mathbf{M}_{aa}$ by the rigid body motion vector $\mathbf{R}_{ja}$ and the measured accelerations $\ddot{\mathbf{u}}_a$ according to:

$$\mathbf{F}_j(\omega) = \mathbf{R}_{ja}\,\mathbf{M}_{aa}\,\ddot{\mathbf{u}}_a(\omega) \tag{15}$$

The accuracy of the mass operator method depends on the number of sensors as well as the quality of the finite element model.

As an alternative to the above techniques, a new method to determine effective mass has been recently

developed by Thales Alenia Space and Top Modal. Based solely on measurements, it involves combining a base excitation test with an additional test using an impact hammer or small shaker test. The additional test provides the force measurement needed to obtain the effective masses.

To explain the new method, consider the expression for the effective mass in Eq. (13). Replacing the vector of participation factors by the vector of effective transmissibilities leads to the following expression for the effective masses defined as a function of the effective transmissibilities and effective flexibilities.

$$\tilde{\mathbf{M}}_{jj,k} = \frac{\tilde{\mathbf{T}}_{ji,k}\ \tilde{\mathbf{T}}_{ij,k}}{\omega_k^2\ \tilde{\mathbf{G}}_{ii,k}} \qquad (16)$$

Eq. (16) expresses the entire effective mass matrix for mode *k* in terms of the drive-point effective flexibility $\tilde{\mathbf{G}}_{ii,k}$ and the corresponding vector of effective transmissibilities $\tilde{\mathbf{T}}_{ij,k}$.

From an experimental point of view, the effective transmissibilities are obtained from the base excitation test whereas the drive-point effective flexibilities are provided by the additional impact hammer test using one of the existing sensor locations as the drive-point.

The effective transmissibilities and flexibilities are obtained from the respective FRF using standard modal identification tools such as the RTMVI method [2] implemented in PRIMODAL [3].

One advantage of this method is that the effective masses can be obtained using the existing instrumentation without any modification to the test fixture. Moreover the additional test with an impact hammer or shaker can be performed any time before or after the base excitation test. Several impact tests can be combined to obtain the effective masses in all three directions. The method assumes that the modes identified from the two tests are consistent in terms of frequency, mode shape and damping. This may not be strictly true in the case of nonlinear behavior of the structure (especially damping) and differences in the boundary conditions between the two tests.

3. INTERFACE LOADS

3.1 Introduction

One of the goals of the study presented in this paper is to estimate loads at the interface of a subsystem (transfer point) from the loads experimentally evaluated at the spacecraft interface (drive point). From the modal superposition theory, the latter ones are computed by considering the effective masses of all the modes contained in the relevant frequency band. By the proposed approach, they are evaluated at the main resonance of a subsystem using the effective mass of the single mode evaluated experimentally by Eq. 16. The spacecraft is therefore assumed to behave like a SDOF system at each mode. To fulfill this assumption, the following conditions have to be satisfied:

1. The mode in question must be weakly coupled with nearby modes.
2. It must be a pure subsystem mode, without any participation of other S/C components.

It can be demonstrated that the first condition can however be relaxed if nearby modes have low effective masses in order to not alter the main contribution to S/C interface loads coming from relevant subsystem resonance. Inversely, the second condition must be fully satisfied since, when two or more subsystems of a spacecraft resonate at the same frequency, it is not possible to discriminate the contributions of each subsystem from the S/C interfaces loads. This is however possible by analysis using MSC.Nastran v2018 which enables to compute effective mass per subsystem.

3.2 S/C Interface Loads

By modal superposition, the S/C interface force F_j^{drive} and moment $M_{\bar{j}}^{drive}$ along the driven axis are computed by:

$$F_j^{drive}(\omega) = \left(\sum_{k=1}^{N} T_k(\omega) * \tilde{M}_{jj,k}\right) * \ddot{u}_j(\omega) \qquad (17)$$

$$M_{\bar{j}}^{drive}(\omega) = \left(\sum_{k=1}^{N} T_k(\omega) * \tilde{M}_{j\bar{j},k}\right) * \ddot{u}_j(\omega) \qquad (18)$$

where:

- $\tilde{M}_{jj,k}$ = effective mass of mode k
- $\tilde{M}_{j\bar{j},k}$ is the term $j\bar{j}$ of the effective mass matrix.
- $\ddot{u}_j$ = drive point input acceleration
- T_k = SDOF transmissibility function (Eq. 10)

Eq. 17 accounts for the dynamic mass contributions of a truncated modal base containing N modes. It is recalled that, for each mode extracted by modal analysis, a full [6x6] matrix is computed. It contains dynamic mass (force/acc.) and inertia (moment/angular acc.) terms and cross-terms (moment/acc.). As the modal mass term related to the translation along the driven axis can be evaluated by performing one sine sweep and one impact test, the cross-axis term needs additional impact tests. In the frame of the main application case reported later in the paper, the moment was evaluated using the effective mass but by introducing the modal center of gravity $h_{k,j}$:

$$M_{\bar{j}}^{drive}(\omega) = \sum_{k=1}^{N} T_k(\omega) * \tilde{M}_{jj,k} * h_{k,j}^{CoG} * \ddot{u}_j(\omega) \qquad (19)$$

Analytically, modal center of gravity (CoG) can be evaluated for each mode through the square root of the ratio between effective inertia and mass. This method presents the main disadvantage of using effective inertia which is related to the angular acceleration at the spacecraft base. Another formulation was needed during the test to evaluate the modal Cog and another approach whose validity was confirmed in the frame of the Instrument test discussed later was found. It was evaluated at the resonance ω_r using internal response measurements as the center of acceleration by:

$$h_{k,j}^{CoG} = \sum_{n=1}^{P} h_n * a_{n,j}(\omega_r) / \sum_{n=1}^{P} a_{n,j}(\omega_r) \qquad (20)$$

where P is the number of accelerometers installed on the subsystem for the test. As a main result of the present study, it is demonstrated that, at a S/S mode frequency and under specific assumptions, modal superposition is not needed and the interface shear force and bending moment are driven solely by the effective mass of the resonant subsystem. Eqs 17-19 simplify then as follows:

$$F_j^{drive}(\omega_r) \cong Q_r * \tilde{M}_{jj,r} * \ddot{u}_j(\omega_r) \qquad (21)$$

$$M_j^{drive}(\omega_r) \cong Q_r * \tilde{M}_{jj,r} * \ddot{u}_j(\omega_r) * h_{r,j}^{CoG} \qquad (22)$$

For a given mode, the interface force at drive point depends on damping (Q_r factor), effective mass and base acceleration while the moment depends also on modal center of gravity.

3.3 S/S Interface Loads

When generated by a single subsystem, with no other spacecraft structural item involved, the S/C interface loads can be considered as acting directly at the subsystem interface. To demonstrate this load equivalence, the equations of motion are written differently from the usual way based on large mass acceleration input.

For instance, the equation along the j-axis of the S/C can be written assuming the resultants of the inertia, viscous and elastic loads acting on spacecraft are "statically" balanced by the spacecraft/shaker interface loads for each frequency step swept by sine excitation.

$$F_j^{drive} = M\ddot{u}_j + B\dot{u}_j + Ku_j \qquad (23)$$

M, B and K are respectively the mass, modal damping and stiffness and matrices of the S/C as $u_j, \dot{u}_j, \ddot{u}_j$ the internal displacement, velocity and acceleration vectors. From elasticity theory, the static equilibrium condition of a system is still ensured if one of its parts, or subsystems, is removed and replaced by the equivalent resultant forces and moments applied to interface. Replacing the *P* subsystems of a spacecraft by their resultants $F_{j,m}$ and denoting *n* the resonant subsystem, the resultant along the direction j force at drive point assumes the following form:

$$F_j^{drive}(\omega) = F_{j,n}(\omega) + \sum_{\substack{m=1 \\ m \neq n}}^{P} F_{j,m}(\omega) \qquad (24)$$

The contributions of the un-deformed structures can be gathered under the term R_j which is proved to be very small compared to the contribution related to the modal mass of the resonant subsystem.

$$R_j(\omega_r) = \sum_{\substack{m=1 \\ m \neq n}}^{P} F_{j,m}(\omega_r) \ll F_{j,n}(\omega_r) \qquad (25)$$

This allows demonstrating the load equivalence between the S/C base and the resonant S/S interface.

$$F_j^{drive}(\omega_r) \cong F_{j,n}(\omega_r) \qquad (26)$$

Concerning the bending moment, Eq. 26 is rearranged for taking into account two contributions for each subsystem. The first one is related to the moment generated by the subsystem at its interface and the second one due to the force times the arm h_n corresponding to the distance between the transfer and drive points. Neglecting the contributions of the un-deformed structures in front of the moments generated by the moving mass of subsystem *n* we have:

$$M_j^{drive}(\omega_r) \cong M_{j,n}(\omega_r) + h_n * F_{j,n}(\omega_r) \qquad (27)$$

Moreover, if the arm h_n is small enough, like for the full instrument application case, the force contribution becomes negligible and Eq. 11 simplifies further taking on the same form of Eq. 10.

$$M_j^{drive}(\omega_r) \cong M_{j,n}(\omega_r) \qquad (28)$$

Using Eqs 23-24, the subsystem interface force and moment at resonance frequency become:

$$F_{j,n}(\omega_r) \cong Q_r * \tilde{M}_{jj,r} * \ddot{u}_j(\omega_r) \qquad (29)$$

$$M_{j,n}(\omega_r) \cong Q_r * \tilde{M}_{jj,r} * h_{r,j}^{CoG} * \ddot{u}_j(\omega_r) \qquad (30)$$

3.4 Validation by Analysis

The entire approach including experimental effective mass computation and subsystem interface load estimation was validated by demonstrating by analysis the following points:

- ❑ Effective mass formulation (Eq. 16)
- ❑ I/F loads computation by modal superposition
- ❑ Load equivalence between S/C and S/S I/Fs
- ❑ SDOF approximation for S/S I/F load estimation

The spacecraft model used to perform the relevant analyses is schematically shown in Fig. 3.

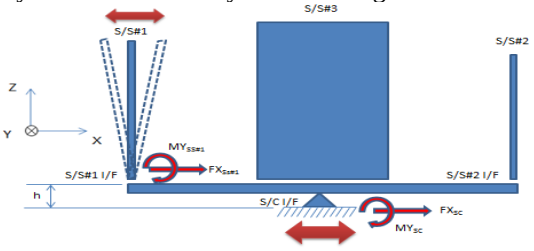

Figure 3 : S/C model used for approach validation

It consists of a support panel carrying three main subsystems and its modal behavior is such that the main modes of each subsystem are uncoupled from those of the other subsystems. Nevertheless, the modal basis of the whole spacecraft is enriched by modes of smaller components and units which can alter the responses of the three subsystems.

❑ *Effective Mass Formulation*

To validate Eq. 16 two sine analyses were performed: the first one imposing 3-axis unit sine accelerations at S/C base and the second one injecting a unit load sine input on a dedicated point of the Subsystem#1. The latter analysis was aimed to simulate an impact test performed with a portable mini-shaker and was preferred, for practical issues, to transient analysis simulating a hammer impact test. Impact and sine test FRFs of the selected point are shown respectively in Fig. 4 and Fig. 5.

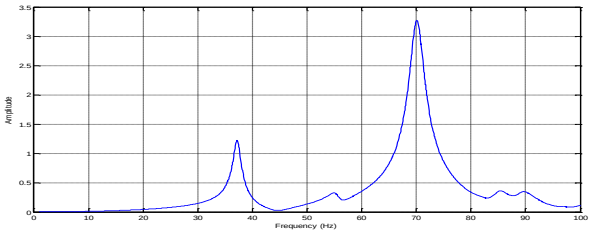

Figure 4: Impact test FRF

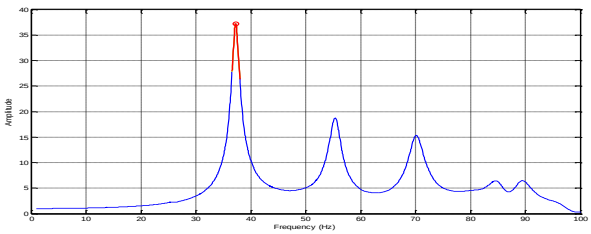

Figure 5: Sine test FRF

The effective transmissibilities and flexibilities were identified using PRIMODAL. The IDEN module (Fig. 6) dedicated to modal identification was used to determine the natural frequency, damping and effective parameters (MEP) from the FRF computed by MSC.Nastran.

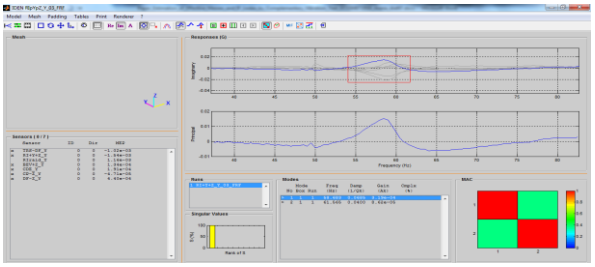

Figure 6 : PRIMODAL Iden module window view

The modal parameters were then combined using Eq. 16 to compute the effective mass given in Tab. 1.

	Primodal	**MSC.Nastran**
Frequency (Hz)	37.2	37.2
Eff. Transmissibility $\widetilde{\mathbf{T}}_{\mathbf{ij,k}}$	1.48	
Eff. Flexibility $\widetilde{\mathbf{G}}_{\mathbf{ij,k}}$ ($Kg^{-1}s^2$)	5.7E-6	
Eff. Mass $\widetilde{\mathbf{M}}_{\mathbf{jj,k}}$ (Kg)	44.3	45.6

Table 1 : MEPs obtained by numerical simulations

The effective mass computed by MSC.Nastran modal analysis is less than 3% higher.

❑ *I/F Load Computation by Modal Superposition*

Eqs 17-19 were validated by comparing the interface forces computed using MSC.Nastran to ones computed by a program coded in MATLAB. MSC.Nastran SOL111 was used to compute the interface forces of the S/C finite element model excited by 3-axis unit sine sweeps. The MATLAB program used the modal base extracted by MSC.Nastran in the relevant frequency band for superposing the contribution of all modes. Residual vectors, included by default in the MSC.Nastran simulation, were also taken into account and modal damping was set to 2% for the entire frequency band for both simulations. Forces and moments issued from X-axis lateral excitation are perfectly superimposed. The moment computed using the modal CoG given by Eq. 20 provides good correlation, in particular at the main resonance frequency as shown in Fig. 7.

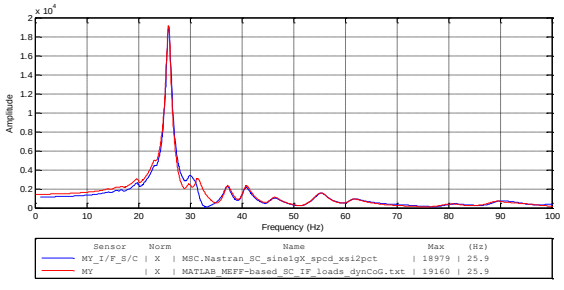

Figure 7 : S/C I/F Moment (Nastran vs Matlab)

❑ *Load Equivalence between S/C and S/S I/Fs*

The third main assumption to be validated concerned the load equivalence between S/C and S/S interfaces.

For this purpose, numerical simulations were performed using only MSC.Nastran. For the X-axis base excitation, S/C interface loads are compared to the ones at the interface of the Subsystem#1 in Fig. 8 and Fig. 9. At the first mode frequency (~37 Hz), the subsystem lateral force and bending moment are slightly lower than the S/C ones, respectively of 13% and 24%. These differences are due to the presence of the nearby mode at 41 Hz whose contribution alters the loads due to subsystem pure resonance.

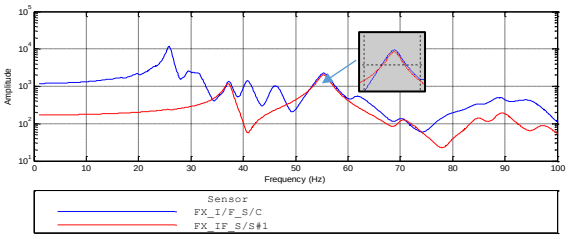

Figure 8 : S/C & S/S I/F Forces (Nastran) - X

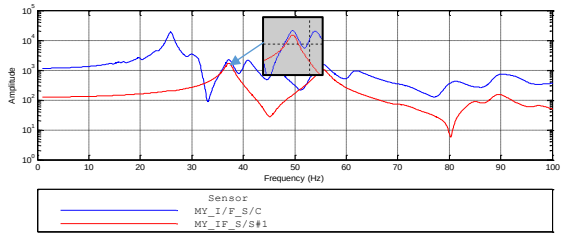

Figure 9 : S/C & S/S I/F Moments (Nastran) – X

Along the Y-axis the mode occurs at 53 Hz and is not coupled with any other one. In this case forces are exactly the same whilst moments differ by less than 4%. The results for the two driven axes are summarized in Tab. 2.

Drive	Freq.	Load	S/C I/F (Nastran)	S/S#1 I/F (Nastran)	Δ
X	37 Hz	F_X [daN]	1355	1178	-13.1%
		M_Y [daNm]	2259	1709	-24.3%
Y	55 Hz	F_Y [daN]	2837	2839	+0.1%
		M_X [daNm]	3317	3187	-3.9%

Table 2 : S/C & S/S interface loads

These examples highlight clearly the importance of the assumptions made in §3.1 about the mode coupling and indicate that their relevance depends on the proximity of the nearby modes and their effective masses as well.

❑ *SDOF approximation for S/S I/F load estimation*

The SDOF approximation was validated by evaluating interface loads using Eqs 15-16 for both lateral excitations and comparing them to those obtained by MSC.Nastran (see Tab. 3).

Drive	Freq.	S/S#1 I/F	Nastran	SDOF	Δ
X	37 Hz	FX [daN]	1178	1141	-3.1%
		MY [daNm]	1709	2078	+21.6%
Y	55 Hz	FY [daN]	2839	2793	-1.6%
		MX [daNm]	3187	3266	+2.5%

Table 3 : S/S#1 I/F loads (Nastran vs SDOF)

The best results are obtained for the Y-axis where no mode coupling occurs. The SDOF approach leads to an over-estimation of the S/S interfaces loads of only 2.5% in the worst case.

4. BEAM TEST CASE

The computation of the effective mass using the method described in §2 was validated experimentally by means of a simple specimen consisting of a steel beam welded on a plate at one end and carrying a tip mass shown in Fig. 10. By analysis, the first bending mode along the less stiff axis (X) is at 24.5 Hz whereas the second one along the stiffer axis (Y) is at 100.5 Hz.

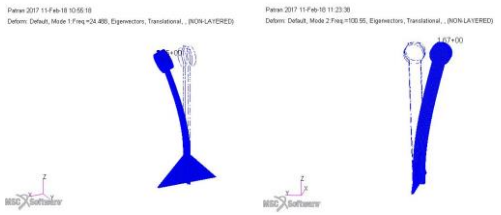

Figure 10: Mode shapes of beam lateral modes

Two mechanical tests were performed:

1. A sine test to determine effective transmissibility.
2. An impact test to determine effective flexibility.

The test configurations and the location of the accelerometers installed on beam are shown in Fig. 11.

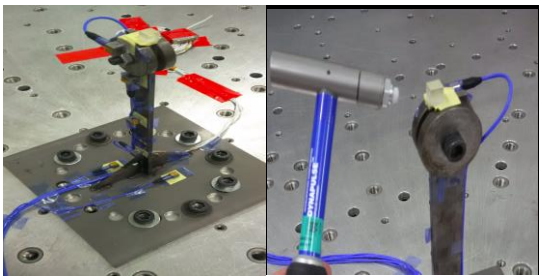

Figure 11: Beam sine and impact test configurations

Being the most common and practical method, an impact hammer was used to apply the pulse excitation. The choice of the hammer tip is usually driven by the specimen mode frequencies to be excited. Indeed, the frequency content of the energy applied to the structure is mainly a function of the stiffness of the contacting surfaces. This stiffness affects the shape of the pulses which in turn determines the response frequency content. The typical responses associated with the different types of tip are plotted in Fig. 12.

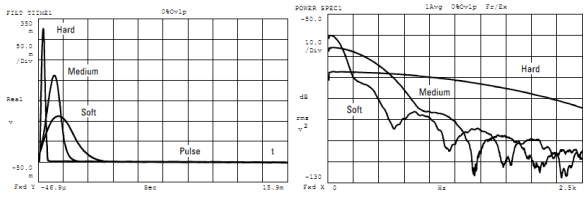

Figure 12: Hammer tips and corresponding responses

In order to obtain the most accurate measurements, soft (rubber) and medium (Teflon) hammer tips were used. However, the Teflon tip produced the noisy results highlighted in Fig. 13 and was hence discarded.

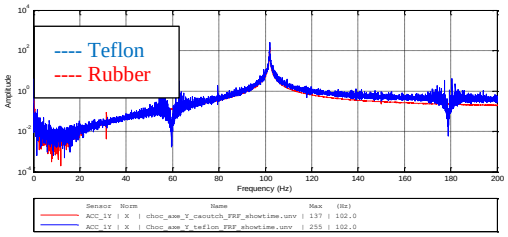

Figure 13 : Soft and medium hammer tip results

Concerning the sine test, the frequency of X-axis mode was not well correlated since the FE analysis underestimated the measured frequency by 23%. This difference was quite surprising for such a relatively simple system. The FRFs were found to be asymmetrical around the peaks thus yielding inconsistent damping values obtained with SINEPOST. Such nonlinear behavior, often encountered with very flexible structure, led to discarding this axis for the effective mass evaluation. For the Y-axis mode, the frequency was well predicted and transmissibility functions had typical symmetrical shapes (Fig. 14).

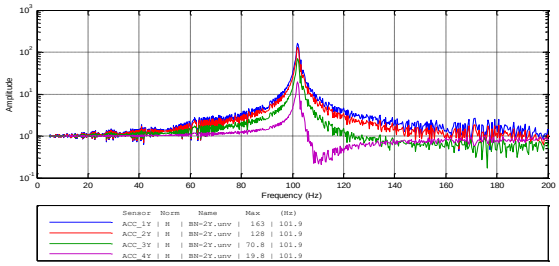

Figure 14 : Y-axis sine test FRFs (beam test case)

The impact test responses were not affected by noise and the mode was correctly identified at 102 Hz. The results of the PRIMODAL modal identifications of both sine sweep and impact tests are summarized in Tab. 4 along with the effective mass comparison.

Test	Freq.	Damping ($1/Q_k$)	MEP $\tilde{T}_{ij,k}$ / $\omega^2\tilde{G}_{ij,k}$
Sine	102.0 Hz	0.0061	-1.06
Hammer	101.9 Hz	0.0014	-2.06 kg^{-1}
Experimental Eff. Mass (Kg)			0.556
FEM Eff. Mass (Kg)			0.562

Table 4 : Effective mass comparaison (beam)

The experimental effective mass was very close to the analytical value so fully validating the method.

5. INSTRUMENT APPLICATION

5.1 Introduction

Following validation by analysis and experimentally through the simple test case application (see §3), the effective mass estimation was then applied to a full scale observation Instrument built by Thales Alenia Space and successfully qualified at the test center in Cannes. As discussed earlier, the general approach was developed with the aim of evaluating the interface loads of two main subsystems during the Instrument sine tests. The two subsystems are basically sandwich panels supported by tubular frames connected to the main supporting structure of the Instrument. For each subsystem, the effective modal parameters were evaluated at the point experiencing the highest modal displacements at the resonances. The mechanical test instrumentation plan was defined accordingly by installing accelerometers on the most suitable locations of the panels.
The load equivalence demonstrated by analysis in §3.1 was used to determine the interface loads and the test strategy was defined accordingly to not exceed the subsystem quasi-static loads. The mass operator method was also implemented for both subsystems since estimating loads with two methods ensured having redundancy and therefore reducing potential errors.

5.3 Impact test set-up

A soft tip was used for two reasons: to better excite the low-frequency modes and to avoid damaging the structure. A Dytran Dynapulse 5850B impact hammer equipped with a force sensor was used. The hammer includes a 3-position toggle switch located on the handle used to select three different sensitivities. The choice of sensitivity depends on the size of the test objects. The hammer was directly connected to the data acquisition system LMS ScadasLab. Although LMS transient acquisition software is not intended for this purpose, it allows recording the throughput of the tests performed with the impact hammer. Moreover, the software allowed selecting the sampling frequency of 2048 Hz for the tests.
Each test was repeated at least twice to ensure obtaining a single impulse force with no rebound. The impact tests were performed in the same spacecraft configuration as the sine test, i.e. on the shaker, in order to have the same boundary conditions. Note that depending on the specimen layout (i.e. lack of accessibility) and test facility constraints (i.e. cleanliness tent) the most suitable point for impact cannot always be chosen, resulting in a compromise that takes into account the above constraints.

5.4 Results

PRIMODAL was used to identify, after each sine run, the effective transmissibility from the FRF of the relevant accelerometer. The same procedure was used for all the impact tests performed. In the frame of the present study, the best results were always obtained

performing modal identification using only the FRF of the selected point for both tests. An alternative solution would be to use the full set of FRFs of the instrumented points, under condition of measuring consistent signal for all accelerometers. The effective mass was evaluated after each sine level run but, for practical issues, only the results related to Low Level (LL) and Qualification Level (QL) runs are reported.

- **X-axis drive / Subsystem#1**

The FRFs measured during the impact and sine tests are respectively shown in Fig. 15 and Fig. 16.

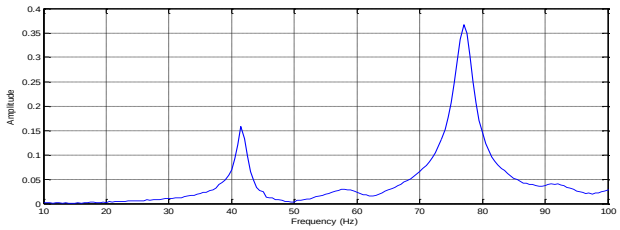

Figure 15 : S/S#1 impact test FRF along X

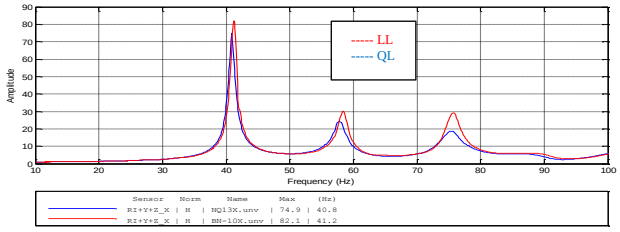

Figure 16 : S/S#1 sine test X FRFs (LL vs QL)

The related modal parameters are reported in Tab. 5.

S/S#1 (X)	Sine LL	Impact Test	Sine QL	Δ
f (Hz)	41.2	41.6	40.8	
Q	55	29	45	
MEP	1.52	0.054 Kg^{-1}	1.66	
M_{eff} (Kg)	43.0	51.3		+19%

Table 5 : S/S#1 effective parameters (X-drive)

The effective mass changes depending on the sine test input level. As usually observed during sine testing, damping increases at qualification level but remains lower than that derived from the impact test. Using Eqs 29-30, the I/F loads are then computed for the qualification run and compared to those obtained with mass operator method for the same run in Tab. 6.

S/S#1 (X)	SDOF	Mass-Op	Δ
Q	45		
M_{eff} (Kg)	51.3		
F_X (daN)	2309	2042	-12%
H_{cog} (m)	1.66	1.50	-12%
M_Y (daNm)	3839	3054	-20%

Table 6 : S/S#1 I/F loads (X-drive)

Notice that the CoG height error and force error are combined to produce the moment error. Concerning the mass operator method, the evaluation of the modal CoG was not needed to determine moments. It was computed afterward by the ratio moment/force and reported only for comparison purposes.

- **X-axis drive / Subsystem#2**

The impact test showed an unusual behavior of the structure (Fig. 17) with two nearby modes instead of the single one observed during the sine sweep (Fig. 18). This affected the PRIMODAL identification leading to inconsistent results for the first peak at 52 Hz, the closest one to the actual resonance frequency.

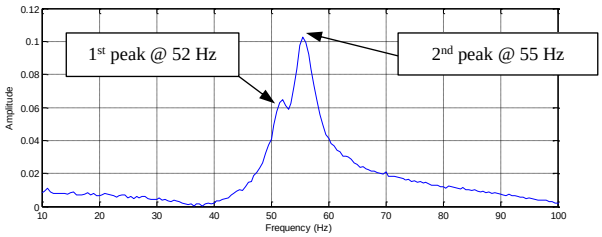

Figure 17 : S/S#2 impact test FRF along X

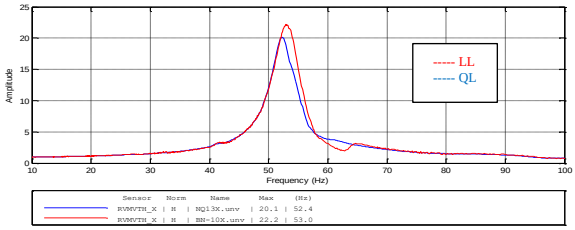

Figure 18 : S/S#2 sine test X FRFs (LL vs QL)

For the second peak, the modal flexibility could be correctly identified resulting in the effective masses given in Tab. 7.

S/S#2 (X)	Sine LL	Impact Test	Sine QL	Δ
f (Hz)	52.6	55.3	52.4	
Q	16	18	16	
MEP	1.74	0.047 Kg^{-1}	1.35	
M_{eff} (Kg)	65.0	39.1		-40%

Table 7 : S/S#2 effective parameters (X-drive)

A significant difference of the effective transmissibility measured during the sine tests was observed. In particular, the low level produced erroneous results since the corresponding effective mass was close to the rigid mass of the subsystem. The results of the intermediate level run were found to be more similar to those of the qualification level. The interface loads are compared in Tab. 8.

S/S#2 (X)	SDOF	Mass-Op	Δ
Q	16		
M_{eff} (Kg)	39.1		
F_X (daN)	606	697	+15%
H_{cog} (m)	1.18	1.04	-12%
M_Y (daNm)	713	728	+2%

Table 8 : S/S#2 I/F loads (X-drive)

Unlike Subsystem#1, mass operator method over-estimates the shear force given by the SDOF approach as the moment is almost the same.

- **Y-axis drive / Subsystem#1**

The modal parameters are reported in Tab. 9.

S/S#1 (Y)	Sine LL	Impact Test	Sine QL	Δ
f (Hz)	55.9	58.7	55.8	
Q	27	15	14	
MEP	1.0	0.0157 Kg^{-1}	1.26	
M_{eff} (Kg)	63.7	101.2		+59%

Table 9 : S/S#1 effective parameters (Y-drive)

The interface loads are given in Tab. 10 showing that mass operator over-estimates SDOF approach.

S/S#1 (Y)	SDOF	Mass-Op	Δ
Q	14		
M_{eff} (Kg)	101.2		
F_Y (daN)	1419	1668	+18%
H_{cog} (m)	0.99	1.06	+7%
M_X (daNm)	1399	1765	+26%

Table 10 : S/S#1 I/F loads (Y-drive)

- **Y-axis drive / Subsystem#2**

The related modal parameters are reported in Tab. 11.

S/S#2 (Y)	Sine LL	Impact Test	Sine QL	Δ
f (Hz)	42.8	43.4	41.4	
Q	21	10	12	
MEP	1.01	0.038 Kg^{-1}	1.33	
M_{eff} (Kg)	26.9	46.6		+73%

Table 11 : S/S#2 effective parameters (Y-drive)

The interface loads are given in Tab. 12.

S/S#2 (Y)	SDOF	Mass-Op	Δ
Q	12		
M_{eff} (Kg)	46.6		
F_Y (daN)	548	835	+52%
H_{cog} (m)	1.09	1.02	-6%
M_X (daNm)	597	851	+43%

Table 12 : S/S#2 I/F loads (Y-drive)

The interface loads derived by using the sine low level results are very similar. This occurs as a result of the same increase of both effective mass and damping. A similar situation was observed for S/S#1 under X-axis excitation.

6. CONCLUSIONS

The new method for determining effective masses has been validated using a simple beam structure using its mode along the stiffer axis. Along the other lateral axis the sine responses showed a nonlinear behaviour leading to incorrect modal identification. Applied to the Instrument, a more complex structure, the new technique worked well in most cases. However, for one of the subsystems, the impact test provided inconsistent results along the less stiff axis thus leading to inconsistent results.

Regarding interface loads, some discrepancies using the mass operator method were observed. The mass operator method was established using an uncorrelated FE model which was found to be more flexible than the actual specimen leading to inconsistencies in the mathematical representation most likely affecting the mass operator results. Nevertheless, the sine test strategy took into account such differences in a conservative way, thus allowing to successfully qualifying the Instrument.

The robustness of the full approach depends strongly on the proper implementation of the impact test and the quality of the measurements for both tests. Several impact tests for each direction must be performed to cope with uncertainties related to impact location, signal acquisition parameters and reliability. The type of structure also plays an important role since a simple specimen can lead to the same problems as a complex structure. The test execution should also take into account test facility constraints and specimen layouts.

7. ABBREVIATIONS AND ACRONYMS

CoG	Centre of Gravity
FE	Finite Element
FRF	Frequency Response Function
I/F	Interface
LL	Low Level
MEP	Modal Effective Parameter
Q_k	Amplification factor for mode k
QL	Qualification Level
S/C	Spacecraft
SDOF	Single Degree of Freedom
S/S	Subsystem
T	SDOF system transmissibility function

8. REFERENCES

1. Girard, A., Roy, N., *Structural Dynamics in Industry*. John Wiley & Sons, 2008.
2. Lefevre Y.M., Bonetti J.C., Girard A., Roy N., Calvi A., *Real Time Modal Identification Techniques for Improved Satellite Vibration Testing*, Proceedings, European Conference on Spacecraft Structures, Materials and Mechanical Testing, Toulouse, France, Dec. 2002.Spacecraft mechanical loads analysis handbook, ECSS-E-HB-32-26A, 19 February 2013
3. PRIMODAL User's Manual, Version 2.9, December 18 2017.